

Article

Controlling the S1 Energy Profile by Tuning Excited-State Aromaticity

Ryota Kotani, Li Liu, Pardeep Kumar, Hikaru Kuramochi, Tahei Tahara,
 Pengpeng Liu, Atsuhiko Osuka, Peter B. Karadakov, and Shohei Saito

J. Am. Chem. Soc., **Just Accepted Manuscript** • DOI: 10.1021/jacs.0c05611 • Publication Date (Web): 10 Aug 2020

Downloaded from pubs.acs.org on August 10, 2020

Just Accepted

“Just Accepted” manuscripts have been peer-reviewed and accepted for publication. They are posted online prior to technical editing, formatting for publication and author proofing. The American Chemical Society provides “Just Accepted” as a service to the research community to expedite the dissemination of scientific material as soon as possible after acceptance. “Just Accepted” manuscripts appear in full in PDF format accompanied by an HTML abstract. “Just Accepted” manuscripts have been fully peer reviewed, but should not be considered the official version of record. They are citable by the Digital Object Identifier (DOI®). “Just Accepted” is an optional service offered to authors. Therefore, the “Just Accepted” Web site may not include all articles that will be published in the journal. After a manuscript is technically edited and formatted, it will be removed from the “Just Accepted” Web site and published as an ASAP article. Note that technical editing may introduce minor changes to the manuscript text and/or graphics which could affect content, and all legal disclaimers and ethical guidelines that apply to the journal pertain. ACS cannot be held responsible for errors or consequences arising from the use of information contained in these “Just Accepted” manuscripts.

Controlling the S_1 Energy Profile by Tuning Excited-State Aromaticity

Ryota Kotani,[†] Li Liu,[‡] Pardeep Kumar,^{‡,§} Hikaru Kuramochi,^{‡,§,||} Tahei Tahara,^{‡,§,*} Pengpeng Liu,[†] Atsuhiko Osuka,[†] Peter B. Karadakov,^{⊥,*} and Shohei Saito^{†,||,*}

[†]Graduate School of Science, Kyoto University, Kitashirakawa Oiwake, Sakyo, Kyoto 606-8502, Japan

[‡]Molecular Spectroscopy Laboratory, RIKEN, 2-1 Hirosawa, Wako 351-0198, Japan

[§]Ultrafast Spectroscopy Research Team, RIKEN Center for Advanced Photonics (RAP), 2-1, Hirosawa, Wako 351-0198, Japan

^{||}PRESTO, Japan Science and Technology Agency (JST), Kawaguchi, Saitama, Japan

[⊥]Department of Chemistry, University of York, Heslington, York, YO10 5DD, U.K.

ABSTRACT: The shape of the lowest singlet excited state (S_1) energy profile is of primary importance in photochemistry and related materials science areas. Here we demonstrate a new approach for controlling the shape of the S_1 energy profile which relies on tuning the level of excited-state aromaticity (ESA). In a series of fluorescent π -expanded oxepins, the energy decrease accompanying the bent-to-planar conformational change in S_1 becomes less pronounced with lower ESA levels. Stabilization energies following from ESA were quantitatively estimated to be 10–20 kcal/mol using photophysical data. Very fast planarization dynamics in S_1 was revealed by time-resolved fluorescence spectroscopy. The time constants were estimated to be shorter than 1 ps, regardless of molecular size and level of ESA, indicating barrierless S_1 planarization within the oxepin series.

INTRODUCTION

The shape of the S_1 energy profile is important in the design of photofunctional molecules. For example, the properties and functions of photochromic compounds,¹ molecular rotors,² and excited-state intramolecular proton transfer (ESIPT) dyes³ are critically dependent on subtle differences in the S_1 energy profiles. Therefore, chemical approaches to tuning the shape of the S_1 energy profile are invaluable for controlling the performance of photoreponsive materials,⁴ environment-sensitive fluorescent probes,⁵ and in other applications. Conventionally, this has been achieved by introducing electron-donating/withdrawing substituents,⁶ changing aromatic rings,⁷ replacing heteroatoms,⁸ providing internal steric constraints,⁹ etc. Here we propose a new conceptual approach for controlling the shape of the S_1 energy profile based on tuning the level of excited-state aromaticity (ESA).

The theory of ESA was proposed by Baird in 1972¹⁰ and now the significant role of ESA in various photofunctional systems has gained wide acceptance.¹¹ Nevertheless, experimental evaluation of the quantitative energetics of ESA has been very limited,¹² and there are no reports on tuning the level of ESA for adjusting the S_1 downhill change from bent to planar conformations. To demonstrate this concept, we focused on the excited-state planarization behavior of dibenz[*b,f*]oxepin (**1**),¹³

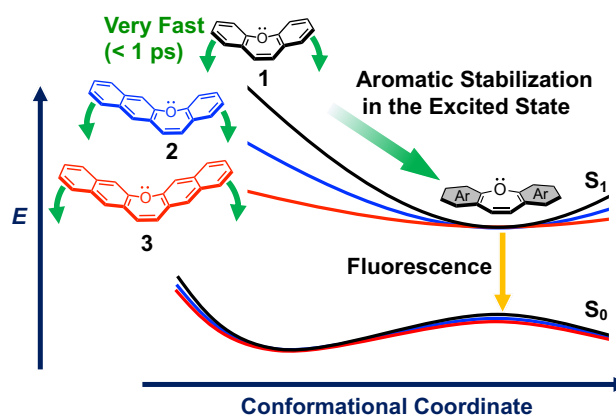


Figure 1. Excited-state aromatization of π -expanded oxepins.

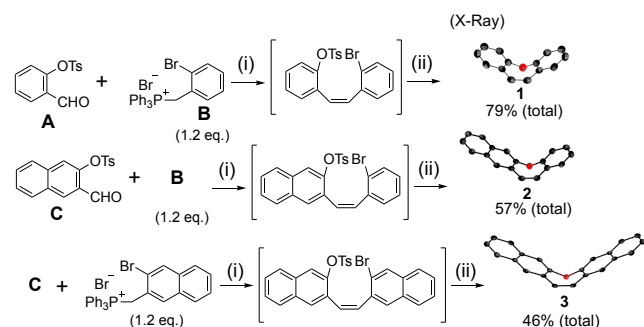
whose aromaticity in S_1 , as well as in T_1 , has been predicted theoretically.¹⁴ The fluorescence (FL) properties of **1** which exhibits a large Stokes shift provide a clear starting point for discussing ESA energetics. Similar planarization dynamics have recently been studied in a series of flapping fluorophores bearing π -expanded cyclooctatetraene (COT),¹⁵ dihydrophenazine,¹⁶ phenothiazine¹⁷ and dibenzoarsepin.¹⁸ However, the S_1 energy profiles of these fluorophores have double (or multiple) minima potentials due to electronic configuration switching during the structural planarization, which makes it difficult to

discuss the effect of ESA.^{15a} In addition, the more popular COT system shows undetectable or faint FL when it has a single minimum S₁ energy profile (Figures S46–53). Therefore, for the current study we selected an emissive oxepin system and developed a new series of π -expanded oxepins. Spectroscopic analyses and theoretical calculations demonstrate that the shape of the S₁ energy profile changes significantly with the level of ESA (Figure 1). Very fast planarization dynamics in S₁ was observed by time-resolved FL spectroscopy, which suggests that these oxepins exhibit barrierless S₁ energy profiles. It should be noted that most of the existing research on ESA is focused on T₁, which is much easier to access computationally in comparison to S₁ that we study here.

RESULTS AND DISCUSSION

Synthesis and Structural Characterization. Three π -expanded oxepins: **1**, benzo[*b*]naphtho[2,3-*f*]oxepin (**2**) and dinaphtho[2,3-*b*:2',3'-*f*]oxepin (**3**) were synthesized (Scheme 1). Precursors of bromoaryl phosphonium ylide and tosyl-substituted aryl aldehyde were coupled by the Wittig reaction, and thus two aryl rings were bridged with a *cis*-olefin. After deprotection of the tosyl group, nucleophilic aromatic substitution was employed to form the oxepin ring. Each of these reactions was performed in a similar way as a one-pot process, giving **1** in 79%, **2** in 57% and **3** in 46% yields based on the aldehyde precursors. X-ray single-crystal structures of **1–3** were obtained showing bent conformations. Bending angles as defined in Figure 5a were observed to be 26.8–27.9° (Figures S1–4), in agreement with those in DFT ground state (S₀) optimized structures (*vide infra*). These angles are significantly smaller than their counterparts in reported COT derivatives (*ca.* 40°),^{15a,19} indicating that π -expanded oxepins feature straighter V-shaped structures. The nonaromatic character of the S₀ bent structures was demonstrated by aromaticity indices (Table S2).

Scheme 1. Synthesis of π -Expanded Oxepins^a



^aConditions: (i) *t*-BuOK (1.4 eq), THF, 0 °C, 30 min then **A** or **C** (1.0 eq), THF, 25 °C, 16 h. (ii) KOH (32 eq), EtOH/H₂O, reflux, 1 h, then K₂CO₃ (4.0 eq), NMP, 120 °C, 20 h. Ts: *p*-Toluenesulfonyl. NMP: *N*-Methylpyrrolidone. In the X-ray crystal structures of **1–3** on the right side, thermal ellipsoids were set to the 50% probability level.

Steady-State Fluorescence Spectra and the Environment Dependence. UV/visible absorption and steady-state FL spectra of **1–3** in CH₂Cl₂ are shown in Figure 2. Upon π -expansion, oxepins **1–3** showed red-shifted absorption peaks (290 nm, 317 nm, and 327 nm, respectively) with increased molar absorption coefficients. FL of **1** was observed at 450, 483, and 516 nm with a characteristic vibronic structure and a remarkably large Stokes shift (12300 cm⁻¹), most probably due to the bent-to-planar conformational change in S₁.¹³ Importantly, we found that the FL peak tops of **1–3** were not shifted despite π -expansion (450 nm for **1**, 449 nm for **2**, and 450 nm for **3** in the shortest FL wavelength). This unshifted FL behavior is unusual in the context of the well-known acene chemistry, where both the absorption and FL spectra are red-shifted with π -expansion.²⁰ Therefore, we expect that there are differences between the S₁ energy profiles of **1–3**. It should be mentioned that, with π -expansion, the FL quantum yields decreased, and the FL lifetimes became shorter (Table 1). This trend is explained by the changes in the nonradiative decay constants *k*_{nr} of the three compounds considering the relatively small differences in the radiative decay constants. Solvent effects in the oxepin series were found to be small, supporting negligible contributions of intramolecular charge transfer in the respective excited-state dynamics (Figures S5–7).

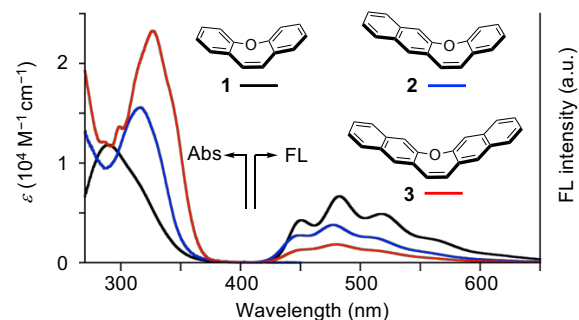


Figure 2. UV/visible absorption and FL spectra of **1–3** in CH₂Cl₂. Excitation wavelength: 280 nm.

Table 1. Photophysical Constants of Oxepins **1–3**

		Φ_F^a	τ_F (ns) ^b	k_r (10 ⁷ s ⁻¹) ^c	k_{nr} (10 ⁷ s ⁻¹) ^d
1	CH ₂ Cl ₂	0.16	10.7	1.5	7.8
	PMMA	0.28	14.9	1.9	4.8
	Crystal	0.31	15.8	2.0	4.4
2	CH ₂ Cl ₂	0.09	6.2	1.5	14
	PMMA	0.16	8.0	2.0	10
	Crystal	0.21	9.1	2.3	8.7
3	CH ₂ Cl ₂	0.04	4.8	0.9	20
	PMMA	0.09	6.5	1.4	14
	Crystal	0.21	7.2	2.9	11

^a FL quantum yield. ^b FL lifetime. ^c Radiative and ^d nonradiative decay rate constants, calculated from Φ_F and τ_F .

We were surprised to observe that the steady-state FL spectra of **1–3** showed no apparent dependence on the viscosity of the DMSO/glycerol mixed solvents (Figure 3a–c), whereas flapping systems studied previously have been reported to exhibit remarkable viscosity responses.^{15c,16c} The apparent viscosity independence can be attributed to the very fast planarization dynamics with a barrierless S₁ energy profile (*vide infra*). Ostensibly, the population of V-shaped species does not accumulate even in viscous media and, therefore, emission from V-shaped species is not observed in the steady-state FL spectra. More importantly, the large Stokes shift of **1** was still observed even in a frozen medium of 2-methyltetrahydrofuran (Figures 3d), most likely because the small structural change from the relatively straight V-shaped form to the planar form is not suppressed, as suggested in the literature for **1**.¹³ On the other hand, blue shifts in the shortest FL wavelengths during the freezing process from –140 to –192 °C became more explicit as the molecular size increases (448 to 445 nm for **1**, 446 to 438 nm for **2**, and 449 to 437 nm for **3**; Figures 3d–f). Since the excitation spectra were not largely shifted during the freezing process (Figures S14, S17, and S20), the Stokes shifts became smaller. This result indicates that, in frozen media, the structural change in the excited state is partially suppressed for the larger molecules **2** and **3**. This tendency was also confirmed in a rigid polymer (PMMA) matrix (Figures 3g–i), although the degree of the structural suppression is still smaller than in the reported

cases of COT-fused anthracene dimers.^{15a,15c} Interestingly, the FL spectrum for microcrystals of **1** was similar to that in solution (Figure 3g). The excitation spectrum was red shifted compared with that in solution (Figure S8), indicating the presence of intermolecular interactions in the ground state. However, the FL wavelengths are not largely shifted, and the clear vibronic structure corresponding to the solution spectrum was observed for the microcrystals, which suggests that the excited-state planarization still occurs in the crystal packing. Whereas large structural changes in molecules are usually thought to be prohibited in the crystalline phase, a considerable number of exceptions have been reported recently in photoresponsive crystals.²¹ To discuss the possibility of the structural planarization in crystals, we have analyzed the distribution of small voids in the crystal packing structures of **1–3**. As a result, small but significant void regions were found near the “flapping wings” of **1–3** (benzene and naphthalene moieties), which may allow the flapping motions. (Figures 4 and S26–28). It is worth noting that the FL spectrum for the microcrystals of **2** is not largely shifted from the solution spectrum (Figure 3h), while the FL spectrum of **3** was significantly blue shifted in crystals (Figure 3i). These results suggest that the excited-state structural change of the large-sized molecule would not provide completely planar geometry in the crystals, even considering the presence of the small voids surrounding the molecule.

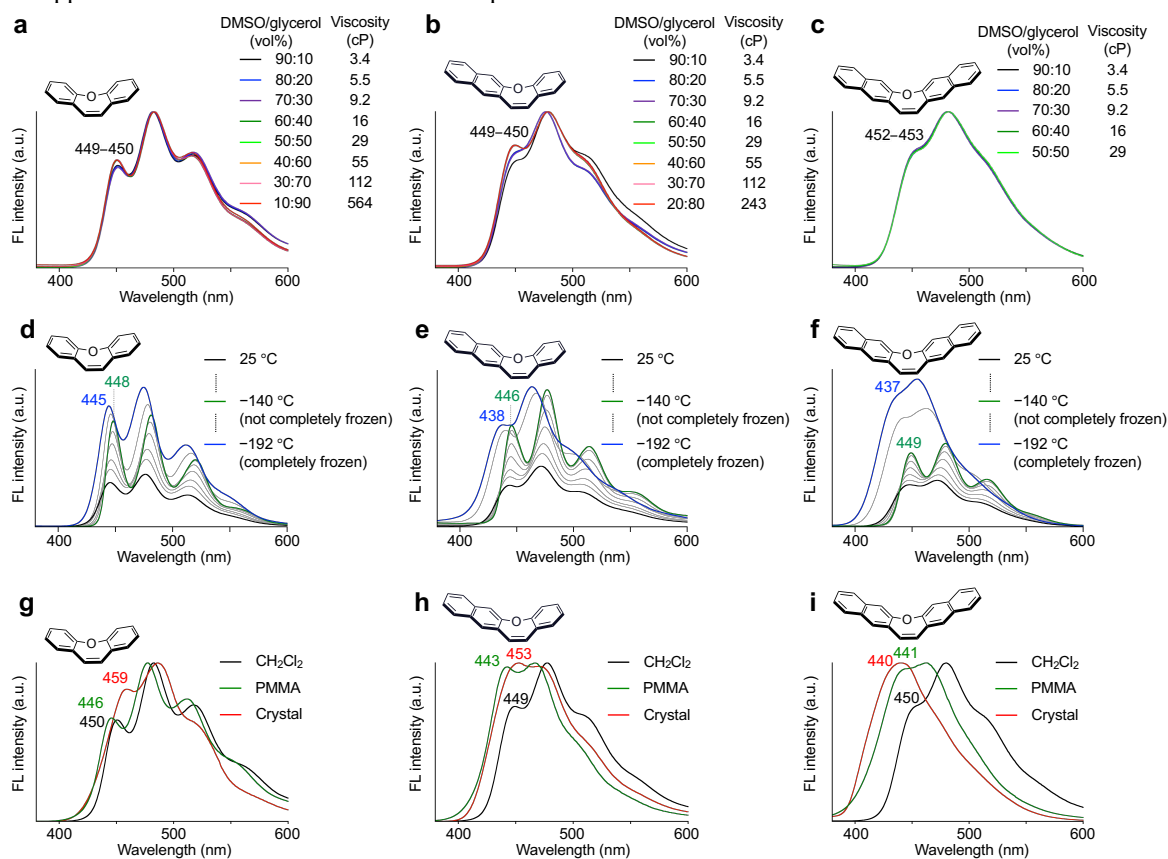


Figure 3. (a–c) FL spectra of **1–3** in DMSO/glycerol mixed solvents at 25 °C. FL spectrum in higher glycerol ratio is not shown due to poor solubility. (d–f) Temperature-dependent FL spectra of **1–3** in 2-methyltetrahydrofuran (2-MeTHF). Note that the melting point of 2-MeTHF is –136 °C. (g–i) FL spectra of **1–3** in CH₂Cl₂ (*ca.* 10^{–6} M, black), a PMMA matrix (0.01 wt% dispersion, green) and microcrystals (as-prepared, red) at 25 °C. Excitation wavelength: 280 nm.

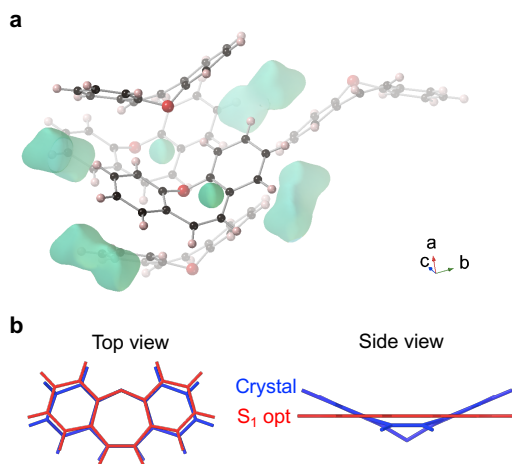


Figure 4. (a) Representation of voids in the crystal packing structure of **1**. Probe radius: 0.65 Å. (b) Superpositions of the X-ray crystal structure (blue) and the S₁ optimized structure at the TD CAM-B3LYP/6-31+G(d) level (red) for **1**.

Energy Profile and Evaluation of Aromaticity. To reveal the reasons for the anomalous unshifted FL behavior in Figure 2, the S₀ and S₁ energy profiles were calculated at the (TD)CAM-B3LYP/6-31+G(d) level, through constrained geometry optimizations at fixed values for the bending angle of the oxepin ring (Figure 5). The bending angle was defined as the dihedral angle between the O–C3–C4 and the O–C1–C2–C3 planes. The S₀ local minimum geometries of **1–3** were found to be V-shaped with bending angles of 25.7–26.9°; planar optimized geometries were found to correspond to transition states of S₀ flapping motion (Figures S23–25). The S₀ inversion barriers are very similar (4.2 for **1**, 3.7 for **2**, 3.6 for **3**, in kcal mol⁻¹). To evaluate aromaticity in S₀ and S₁, further optimizations were performed at the (TD)B3LYP-D3BJ/def2TZVP level, followed by CASSCF(2,2)-GIAO/6-311G(d) NICS calculations at the optimized geometries (Figures S44–45). The (TD)CAM-B3LYP/6-31+G(d) and (TD)B3LYP-D3BJ/def2TZVP geometries are in very good agreement, which suggests that further improvements of the DFT approach are unlikely to introduce significant changes. A singlet CASSCF(2,2) construction can be used to approximate the S₁ wavefunction and calculate S₁ NICS when S₁ is dominated by the HOMO–LUMO transition.²² The S₀ planar transition states of **1–3** are found to be strongly antiaromatic as indicated by several calculated aromaticity indices: HOMHED²³, NICS(1)_{zz}²⁴, and ACID²⁵ (Table 2, Figures S36–41). In S₁, single minimum energy profiles were obtained, with planar optimal geometries of C_{2v} and C_s symmetry, for **1** and **3**, and **2**, respectively (Figures S23–25). According to the results of the S₀ and S₁ calculations, the V-shaped S₀ geometries of **1–3** are all planarized by photoexcitation in S₁. It is important to note that the extent of energy stabilization by planarization is remarkably different between **1–3** (Figure 5). The differences stem from the

significant disparity in the levels of S₁ aromaticity in these compounds which follow the order **1** > **2** > **3**, where stronger S₁ aromaticity was indicated by higher HOMHED and more negative NICS(1)_{zz} values (Table 2). Since the S₁ electronic configurations of the planarized geometries are dominated by the respective HOMO–LUMO transitions (Figure 6), the CASSCF(2,2) method was applied to the estimation of the S₁ NICS values.²² (Moderate oscillator strengths for the S₀–S₁ transitions are consistent with the fluorescent properties of **1–3**.) As a result, π-expansion of oxepins weakens the S₁ aromaticity, providing a flatter energy profile. Accordingly, the lowest harmonic S₁ frequencies, corresponding to the flapping vibrational mode, were obtained as 69 cm⁻¹ for **1**, 46 cm⁻¹ for **2**, and 32 cm⁻¹ for **3** at the TD B3LYP-D3BJ/def2TZVP level.

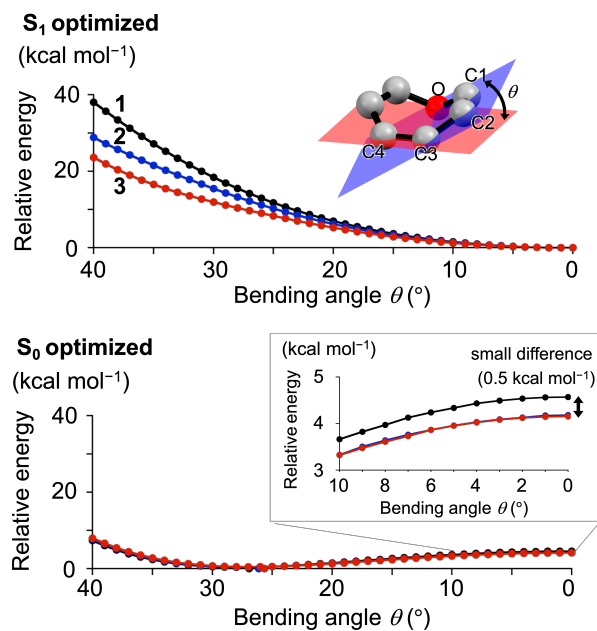


Figure 5. Calculated S₁ and S₀ energy profiles of oxepins **1** (black), **2** (blue), and **3** (red) at the (TD)CAM-B3LYP/6-31+G(d) level. Energies relative to those of the S₁ and S₀ optimized geometries were plotted vs the constrained bending angles.

Table 2. Aromaticity Indices of 1–3 in S₀ (TS) and S₁

	HOMHED (oxepin) ^a		HOMHED (perimeters) ^a		NICS(1) _{zz} (ppm) ^a	
	S ₀	S ₁	S ₀	S ₁	S ₀	S ₁
1	0.676	0.835	0.849	0.926	22.3	–53.2
2	0.685	0.814	0.875	0.932	19.9	–51.5
3	0.686	0.802	0.890	0.942	18.3	–45.6

^aCalculations were performed at planar transition state S₀ geometries and S₁ local minimum geometries obtained at the (TD)B3LYP-D3BJ/def2TZVP level. NICS(1)_{zz} results come from CASSCF(2,2)-GIAO/6-311G(d) calculations.

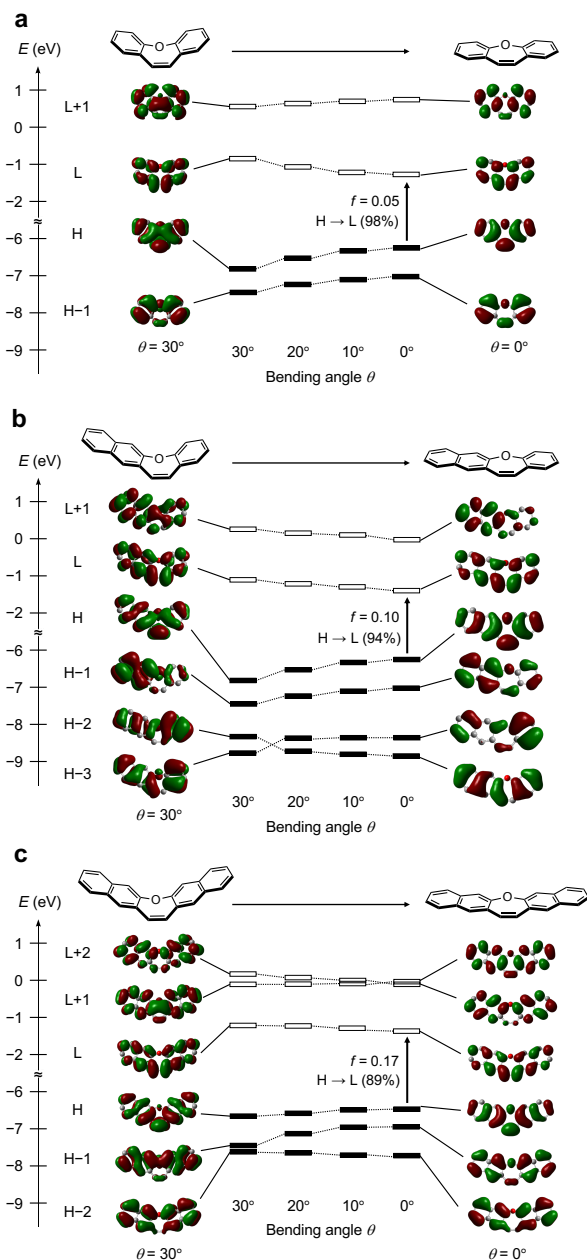


Figure 6. (a–c) Kohn-Sham molecular orbitals and their energies for constrained optimized geometries of **1–3** in S_1 at different bending angles, calculated at the TD CAM-B3LYP/6-31+G(d) level. The two bending angles on the benzene and naphthalene sides were fixed to be equal for **2**. Compositions (%) and oscillator strengths (f) are shown for planar geometries. H and L stand for HOMO and LUMO, respectively.

The shapes of the energy profiles of **1–3** is roughly sketched in Figure 7a. The absorption wavelengths were red-shifted by π -expansion (smaller in energy; purple arrows), whereas unshifted fluorescence was observed (yellow arrows). Since the bent-to-planar energy barriers in S_0 show a small difference for **1–3** (black arrows), the main factor responsible for the unshifted fluorescence

must be different gaps in the S_1 stabilization energies during planarization (green arrows), that is, the differences in the degree of S_1 aromaticity. The relative energies of the S_0/S_1 states at the bent/planar geometries obtained from spectral data (Figure 2) are summarized in Figure 7b. The longest wavelength absorption peak was used to estimate the $S_0 \rightarrow S_1$ vertical transition energy at the S_0 V-shaped geometry, namely, the energy gap between $E(S_0)/S_0$ and $E(S_1)/S_0$ (98.6 for **1**, 90.5 for **2**, and 87.4 for **3**, all in kcal mol⁻¹), while the shortest wavelength FL peak was taken as the $S_1 \rightarrow S_0$ vertical transition energy at the S_1 planar geometry, namely, the energy gap between $E(S_1)/S_1$ and $E(S_0)/S_1$ (63.5 for **1**, 63.7 for **2**, and 63.5 for **3**, all in kcal mol⁻¹). The S_0 energy gap between $E(S_0)/S_0$ and $E(S_0)/S_1$ (15.5 for **1**, 14.4 for **2**, and 13.5 for **3**, all in kcal mol⁻¹) was taken from the CAM-B3LYP/6-31+G(d) calculations. As a result, the bent-to-planar energy gaps in S_1 ($= E(S_1)/S_0 - E(S_1)/S_1$) were estimated to be 19.6 for **1**, 12.4 for **2**, and 10.4 for **3**, all in kcal mol⁻¹. These values can be viewed as stabilization energies gained by S_1 aromaticity and are comparable to those reported for a COT-based 8π system (21–22 kcal mol⁻¹), although the evaluation method is different.¹²

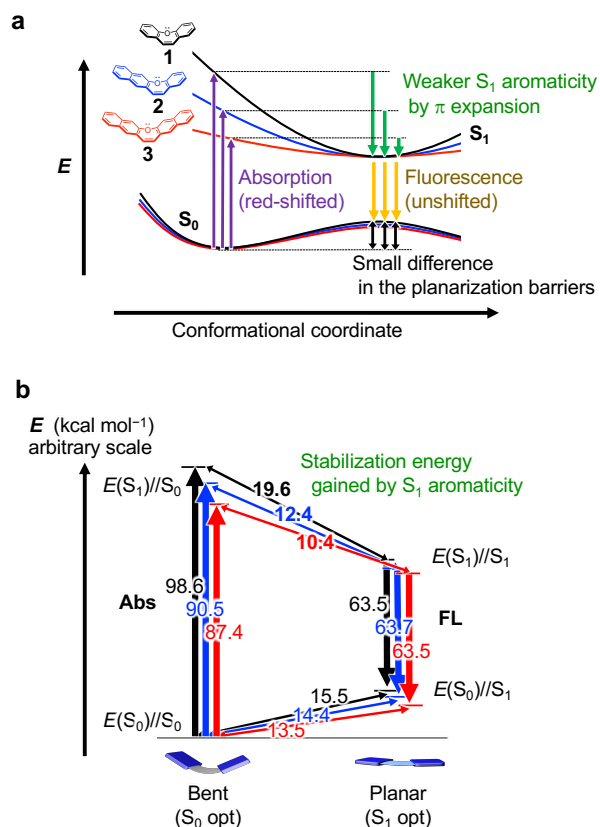


Figure 7. (a) Schematic energy diagrams for **1–3** showing the energy balance for absorption, FL, planarization barriers in S_0 , and excited state aromatization in S_1 . (b) Relative energy levels of the S_0/S_1 states at the bent/planar conformations for **1** (black), **2** (blue), and **3** (red). The energies of vertical transitions were obtained from experimental results.

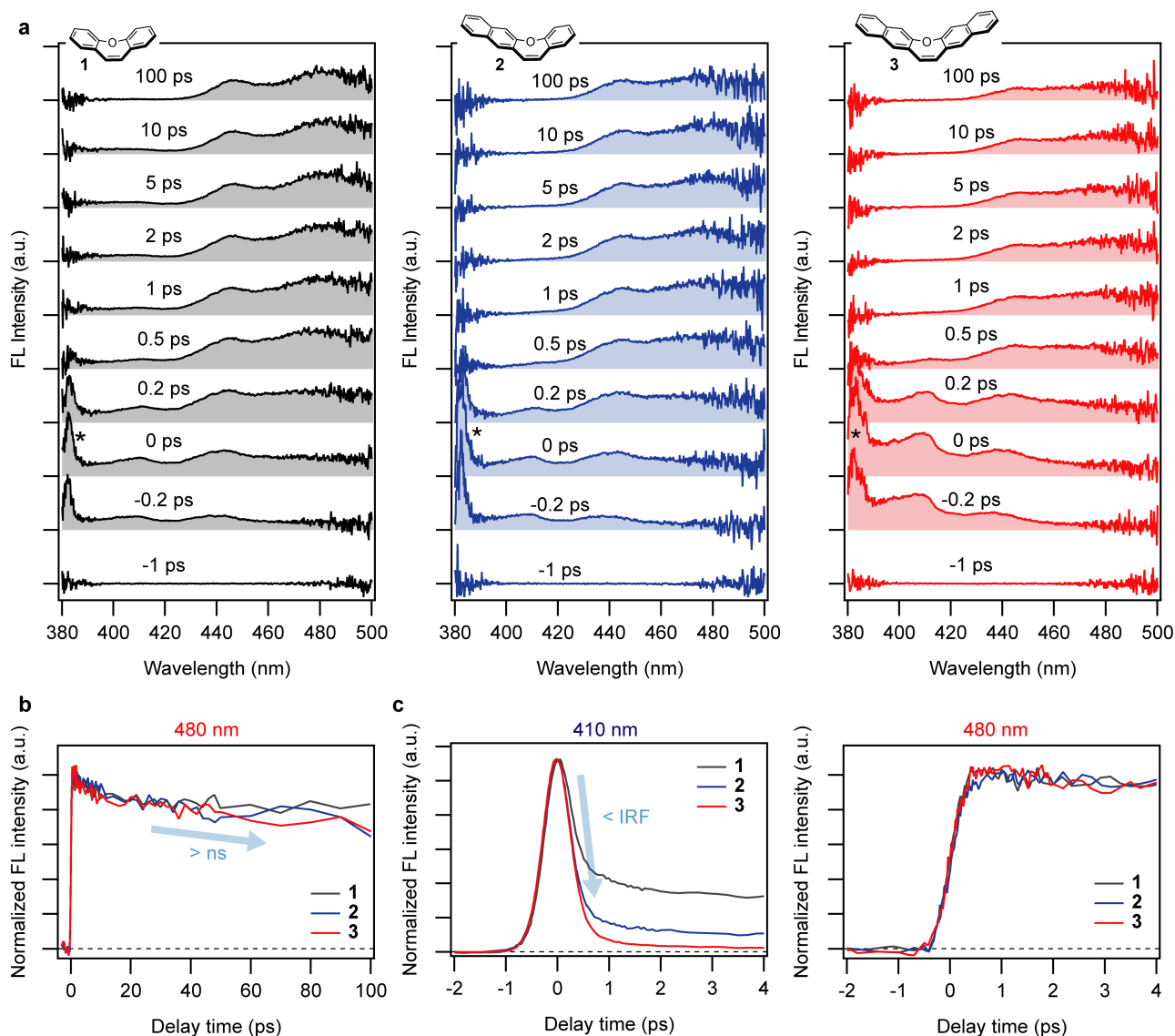


Figure 8. (a) Femtosecond time-resolved FL spectra of **1–3** in CH_2Cl_2 obtained after photoexcitation at 343 nm. The sharp spectral feature at ~ 380 nm denoted by the asterisk is due to the Raman signal of the solvent. (b) Temporal profiles of the time-resolved FL signals at 480 nm. (c) Early time windows of the temporal profiles of the time-resolved FL signals at 410 and 480 nm.

Ultrafast Dynamics. To obtain deeper insights into the planarization dynamics and the S_1 potential energy landscape of **1–3**, we investigated their excited-state dynamics by femtosecond time-resolved FL spectroscopy. Figure 8a shows the time-resolved FL spectra of **1–3** in CH_2Cl_2 upon 343-nm photoexcitation. In all cases of **1–3**, the spectral and temporal behaviors were found to be quite similar. Immediately after photoexcitation (i.e., at 0 ps), a broad FL spectrum with peaks around 410 nm and 445 nm was observed for each of **1–3**. This early time spectrum looks very different from the corresponding steady-state FL spectrum and it is attributed to the FL from the V-shaped conformation. Subsequently, the time-

resolved FL spectrum showed rapid spectral change towards 1 ps, giving rise to a spectral shape almost identical to the steady-state FL spectrum of each sample. Such spectral changes are clearly observable in the time-resolved FL but not in the time-resolved absorption (Figure S54). After 1 ps, the entire FL band decayed slowly on the ns time scale (Figure 8b), in agreement with the FL lifetimes estimated separately (see Table 1).

Our time-resolved FL data clearly show that the V-shaped-to-planar conformational change in **1–3** occurs on the ultrafast time scale. Remarkably, the FL signal of the V-shaped conformation is observed only around the time origin and the FL signal due to the planar conformation (e.g., at 480 nm) rises almost instantaneously as

shown in Figure 8c. These results indicate that the V-shaped-to-planar conformational change in **1–3** is completed within the instrumental response of the setup (~330 fs). This planarization time scale is much shorter than those of other flapping molecules in low viscous media,^{15a-b,16c-d,17} and suggests that the planarization processes of **1–3** are all downhill and barrierless, and proceed continuously on the S₁ potential energy surface.

According to the theoretical calculations shown in Figures 5 and 7, the S₁ state of oxepins has a steeper downhill profile as the molecule becomes smaller. In this case, one would expect faster decay of the V-shaped conformation for the smaller oxepin. Interestingly, the signal around 410 nm looks less pronounced as the molecule becomes smaller. (This is the reason why the temporal evolution of the time-resolved spectrum looks slightly different for **1–3** in Figure 8a.) Although the temporal behaviors are not fully resolved with our time resolution, this result suggests that the lifetime of the V-shaped conformation becomes shorter as the molecule becomes smaller. In other words, it is expected that the planarization time scale is governed by the steepness of the S₁ energy slopes along the planarization coordinate, as the theoretical calculation suggested.

CONCLUSION

In conclusion, we have demonstrated that tuning the level of excited-state aromaticity provides a convenient way of controlling the S₁ energy profiles of photoresponsive molecules. Aromatic stabilization energies were experimentally compared for a series of oxepins, in which further π -expansion was shown to lead to weaker S₁ aromaticity and produce a flatter S₁ downhill planarization energy profile. Systematic studies were conducted to associate the stabilization energies of excited-state aromaticity (19.6 for **1**, 12.4 for **2**, and 10.4 for **3** all in kcal mol⁻¹) with the degree of geometrical and magnetic measures of aromaticity calculated in S₁. Using time-resolved spectroscopies, very fast planarization dynamics (within 1 ps for **1–3**) were observed in all oxepins we studied, despite the differences in molecular size and level of ESA. Changing the degree of the S₁ aromatic stabilization energy can lead to different photoresponses of functional soft materials and supramolecules, because the S₁ aromatization can serve as a driving force for the ultrafast perturbation of their packing structures.^{15b}

ASSOCIATED CONTENT

The Supporting Information is available free of charge on the ACS Publications website. Crystallographic data are also available free of charge from The Cambridge Crystallographic Data Centre, codes 1997512 for **1**, 1997513 for **2** and 1997513 for **3**.

Synthetic protocols, characterization data, photophysical spectra, theoretical calculation (PDF)

AUTHOR INFORMATION

Corresponding Authors

tahei@riken.jp
peter.karadakov@york.ac.uk
s_saito@kuchem.kyoto-u.ac.jp

Funding Sources

This work was supported by JST, PRESTO, Grant Numbers JPMJPR16P6 to S.S. and JPMJPR17P4 to H.K., by JSPS, KAKENHI, Grant Numbers JP18H01952 and JP17H05258 to S.S., by JSPS, Research Fellowship for Young Scientists Grant Number JP18J22477 to R. K.

ACKNOWLEDGMENT

We thank Prof. Dr. Rainer Herges and Fynn Röhrich (Kiel University) for providing us the program of the ACID calculations, and Dr. Kazuya Otsubo (Kyoto University) for advice on the representation of void in the crystal packing.

REFERENCES

- (1) **Photochromic compounds:** (a) Irie, M.; Fukaminato, T.; Matsuda, K.; Kobatake, S. Photochromism of Diarylethene Molecules and Crystals: Memories, Switches, and Actuators. *Chem. Rev.* **2014**, *114*, 12174–12277. (b) *Photochromic Materials: Preparation, Properties and Applications*; Tian, H., Zhang, J., Eds.; Wiley-VCH Verlag: Weinheim, 2016.
- (2) **Molecular rotors:** Sasaki, S.; Drummen, G. P. C.; Konishi, G. Recent advances in twisted intramolecular charge transfer (TICT) fluorescence and related phenomena in materials chemistry. *J. Mater. Chem. C*, **2016**, *4*, 2731–2743.
- (3) **ESIPT dyes:** (a) Sedgwick, A. C.; Wu, L.; Han, H.-H.; Bull, S. D.; He, X.-P.; James, T. D.; Sessler, J. L.; Tang, B. Z.; Tian, H.; Yoon, J. Excited-state intramolecular proton-transfer (ESIPT) based fluorescence sensors and imaging agents. *Chem. Soc. Rev.* **2018**, *47*, 8842–8880. (b) Chen, C.-L.; Chen, Y.-T.; Demchenko, A. P.; Chou, P.-T. Amino proton donors in excited-state intramolecular proton-transfer reactions. *Nat. Rev. Chem.* **2018**, *2*, 131–143.
- (4) **Photoresponsive materials:** (a) Klajn, R. Spiropyran-based dynamic materials. *Chem. Soc. Rev.*, **2014**, *43*, 148–184. (b) Priimagi, A.; Barrett, C. J.; Shishido, A. Recent twists in photoactuation and photoalignment control. *J. Mater. Chem. C* **2014**, *2*, 7155–7162. (c) White, T. J.; Broer, D. J. Programmable and adaptive mechanics with liquid crystal polymer networks and elastomers. *Nature Mater.* **2015**, *14*, 1087–1098. (d) Mutlu, H.; Geislerhart, C. M.; Barner-Kowollik, C. Untapped potential for debonding on demand: the wonderful world of azo-compounds. *Mater. Horiz.*, **2018**, *5*, 162–183. (e) Seki, T. A Wide Array of Photoinduced Motions in Molecular and Macromolecular Assemblies at Interfaces. *Bull. Chem. Soc. Jpn.* **2018**, *91*, 1026–1057. (f) Hohl, D. K.; Weder, C. (De)bonding on Demand with Optically Switchable Adhesives. *Adv. Optical Mater.* **2019**, *7*, 1900230.
- (5) **Environment-sensitive fluorescent probes:** (a) Klymchenko, A. S. Solvatochromic and Fluorogenic Dyes as Environment-Sensitive Probes: Design and Biological Applications. *Acc. Chem. Res.* **2017**, *50*, 366–375; (b) Yang, Z.; Cao, J.; He, Y.; Yang, J. H.; Kim, T.; Peng, X.; Kim, J. S. Macro-/micro-environment-sensitive chemosensing and biological imaging. *Chem. Soc. Rev.* **2014**, *43*, 4563–4601; (c) Kowada, T.; Maeda, H.; Kikuchi, K. BODIPY-based probes for the fluorescence imaging of biomolecules in living cells. *Chem. Soc. Rev.* **2015**, *44*, 4953–4972.
- (6) **Introducing electron-donating/withdrawing substituents:** (a) Beharry, A. A.; Sadovski, O.; Woolley, G. A. Azobenzene Photoswitching without Ultraviolet Light. *J. Am. Chem. Soc.* **2011**, *133*, 19684–19687. (b) Bléger, D.; Schwarz, J.; Brouwer, A. M.;

- Hecht, S. *o*-Fluoroazobenzenes as Readily Synthesized Photoswitches Offering Nearly Quantitative Two-Way Isomerization with Visible Light. *J. Am. Chem. Soc.* **2012**, *134*, 20597–20600.
- (c) Shao, B.; Qian, H.; Li, Q.; Aprahamian, I. Structure Property Analysis of the Solution and Solid-State Properties of Bistable Photochromic Hydrazones. *J. Am. Chem. Soc.* **2019**, *141*, 8364–8371.
- (7) **Changing aromatic rings:** (a) Irie, M.; Mohri, M. Thermally irreversible photochromic systems. Reversible photocyclization of diarylethene derivatives. *J. Org. Chem.* **1988**, *53*, 803–808. (b) Yamashita, H.; Ikezawa, T.; Kobayashi, Y.; Abe, J. Photochromic Phenoxy-Imidazolyl Radical Complexes with Decoloration Rates from Tens of Nanoseconds to Seconds. *J. Am. Chem. Soc.* **2015**, *137*, 4952–4955. (c) Tasaki, S.; Momotake, A.; Kanna, Y.; Sato, T.; Nishimura, Y.; Arai, T. Producing a dual-fluorescent molecule by tuning the energetics of excited-state intramolecular proton transfer. *Photochem. Photobiol. Sci.* **2015**, *14*, 1864–1871.
- (8) **Replacing heteroatoms:** (a) Fu, M.; Xiao, Y.; Qian, X.; Zhao, D.; Xu, Y. A design concept of long-wavelength fluorescent analogs of rhodamine dyes: replacement of oxygen with silicon atom. *Chem. Commun.* **2008**, 1780–1782. (b) Koide, Y.; Urano, Y.; Hanaoka, K.; Piao, W.; Kusakabe, M.; Saito, N.; Terai, T.; Okabe, T.; Nagano, T. Development of NIR Fluorescent Dyes Based on Si–rhodamine for in Vivo Imaging. *J. Am. Chem. Soc.* **2012**, *134*, 5029–5031. (c) Hammerich, M.; Schütt, C.; Stähler, C.; Lenters, P.; Röhricht, F.; Höpner, R.; Herges, R. Heterodiazocines: Synthesis and Photochromic Properties, *Trans to Cis* Switching within the Bio-optical Window. *J. Am. Chem. Soc.* **2016**, *138*, 13111–13114. (d) Wang, C.; Taki, M.; Sato, Y.; Fukazawa, A.; Higashiyama, T.; Yamaguchi, S. Super-Photostable Phosphole-Based Dye for Multiple-Acquisition Stimulated Emission Depletion Imaging. *J. Am. Chem. Soc.* **2017**, *139*, 10374–10381.
- (9) **Providing internal steric constraint:** (a) Kishimoto, Y.; Abe, J. A Fast Photochromic Molecule That Colors Only under UV Light. *J. Am. Chem. Soc.* **2009**, *131*, 4227–4229. (b) Siewertsen, R.; Neumann, H.; Buchheim-Stehn, B.; Herges, R.; Näther, C.; Renth, F.; Temps, F. Highly Efficient Reversible *Z-E* Photoisomerization of a Bridged Azobenzene with Visible Light through Resolved $S_1(\pi\pi^*)$ Absorption Bands. *J. Am. Chem. Soc.* **2009**, *131*, 15594–15595. (c) Fukumoto, S.; Nakashima, T.; Kawai, T. Photon-Quantitative Reaction of a Dithiazolylarylene in Solution. *Angew. Chem. Int. Ed.* **2011**, *50*, 1565–1568.
- (10) **Baird rule:** Baird, N. C. Quantum Organic Photochemistry. II. Resonance and Aromaticity in the Lowest ${}^3\pi\pi^*$ State of Cyclic Hydrocarbons. *J. Am. Chem. Soc.* **1972**, *94*, 4941–4948.
- (11) **Baird aromaticity:** (a) Rosenberg, M.; Dahlstrand, C.; Kilså, K.; Ottosson, H. Excited State Aromaticity and Antiaromaticity: Opportunities for Photophysical and Photochemical Rationalizations. *Chem. Rev.* **2014**, *114*, 5379–5425. (b) Oh, J.; Sung, Y. S.; Hong, Y.; Kim, D. Spectroscopic Diagnosis of Excited-State Aromaticity: Capturing Electronic Structures and Conformations upon Aromaticity Reversal. *Acc. Chem. Res.* **2018**, *51*, 1349–1358. (c) Liu, C.; Ni, Y.; Lu, X.; Li, G.; Wu, J., Global Aromaticity in Macrocyclic Polyradicaloids: Hückel's Rule or Baird's Rule?. *Acc. Chem. Res.* **2019**, *52*, 2309–2321. (d) Rosenberg, M.; Ottosson, H. Kilså, K. Influence of excited state aromaticity in the lowest excited singlet states of fulvene derivatives. *Phys. Chem. Chem. Phys.* **2011**, *13*, 12912–12919. (e) Sung, Y. M.; Yoon, M.-C.; Lim, J. M.; Rath, H.; Naoda, K.; Osuka, A.; Kim, D. Reversal of Hückel (anti)aromaticity in the lowest triplet states of hexaphyrins and spectroscopic evidence for Baird's rule. *Nat. Chem.* **2015**, *7*, 418–422. (f) Oh, J.; Sung, Y. M.; Mori, H.; Park, S.; Jorner, K.; Ottosson, H.; Lim, M.; Osuka, A.; Kim, D. Unraveling Excited-Singlet-State Aromaticity via Vibrational Analysis. *Chem* **2017**, *3*, 870–880. (g) Wu, C.-H.; Karas, L. J.; Ottosson, H.; Wu, J. I-C. Excited-state proton transfer relieves antiaromaticity in molecules. *Proc. Natl. Acad. Sci. USA.* **2019**, *116*, 20303–20308. (h) Wang, J.; Oruganti, B.; Durbeej, B. A Straightforward Route to Aromatic Excited States in Molecular Motors that Improves Photochemical Efficiency. *ChemPhotoChem* **2019**, *3*, 450–460. (i) Bakouri, O. E.; Smith, J. R.; Ottosson, H. Strategies for Design of Potential Singlet Fission Chromophores Utilizing a Combination of Ground-State and Excited-State Aromaticity Rules. *J. Am. Chem. Soc.* **2020**, *142*, 5602–5617.
- (12) **Energetics of ESA:** Ueda, M.; Jorner, K.; Sung, Y. M.; Mori, T.; Xiao, Q.; Kim, D.; Ottosson, H.; Aida, T.; Itoh, Y. Energetics of Baird aromaticity supported by inversion of photoexcited chiral $[4n]$ annulene derivatives. *Nat. Commun.* **2017**, *8*, 346.
- (13) **Oxepin(exp):** Shukla, D.; Wan, P. Evidence for a Planar Cyclically Conjugated 8π System in the Excited State: Large Stokes Shift Observed for Dibenzo[*b,f*]oxepin Fluorescence. *J. Am. Chem. Soc.* **1993**, *115*, 2990–2991.
- (14) **Oxepin(calc):** Toldo, J.; Bakouri, O. E.; Solà, M.; Norrby, P.-O.; Ottosson, H. Is Excited-State Aromaticity a Driving Force for Planarization of Dibenzannelated 8π -Electron Heterocycles. *ChemPlusChem* **2019**, *84*, 712–721.
- (15) **FLAP-COT:** (a) Yamakado, T.; Takahashi, S.; Watanabe, K.; Matsumoto, Y.; Osuka, A.; Saito, S. Conformational Planarization versus Singlet Fission: Distinct Excited-State Dynamics of Cyclooctatetraene-Fused Acene Dimers. *Angew. Chem. Int. Ed.* **2018**, *57*, 5438–5443. (b) Hada, M.; Saito, S.; Tanaka, S.; Sato, R.; Yoshimura, M.; Mouri, K.; Matsuo, K.; Yamaguchi, S.; Hara, M.; Hayashi, Y.; Röhricht, F.; Herges, R.; Shigetani, Y.; Onda, K.; Miller, J. D. Structural Monitoring of the Onset of Excited-State Aromaticity in a Liquid Crystal Phase. *J. Am. Chem. Soc.* **2017**, *139*, 15792–15800. (c) Kotani, R.; Sotome, H.; Okajima, H.; Yokoyama, S.; Nakaïke, Y.; Kashiwagi, A.; Mori, C.; Nakada, Y.; Yamaguchi, S.; Osuka, A.; Sakamoto, A.; Miyasaka, H.; Saito, S. Flapping viscosity probe that shows polarity-independent ratiometric fluorescence. *J. Mater. Chem. C* **2017**, *5*, 5248–5256.
- (16) **Dihydrophenazine:** (a) Zhang, Z.; Song, W.; Su, J.; Tian, H. Vibration-Induced Emission (VIE) of N,N' -Disubstituted-Dihydrobenzo[*a,c*]phenazines: Fundamental Understanding and Emerging Applications. *Adv. Funct. Mater.* **2019**, 1902803. (b) Chen, W.; Chen, C.-L.; Zhang, Z.; Chen, Y.-A.; Chao, W.-C.; Su, J.; Tian, H.; Chou, P.-T. Snapshooting the Excited-State Planarization of Chemically Locked N,N' -Disubstituted-Dihydrodibenzo[*a,c*]phenazines. *J. Am. Chem. Soc.* **2017**, *139*, 1636–1644. (c) Zhang, Z.; Wu, Y.-S.; Tang, K.-C.; Chen, C.-L.; Ho, J.-W.; Su, J.; Tian, H.; Chou, P.-T. Excited-State Conformational/Electronic Responses of Saddle-Shaped N,N' -Disubstituted-Dihydrodibenzo[*a,c*]phenazines: Wide-Tuning Emission from Red to Deep Blue and White Light Combination. *J. Am. Chem. Soc.* **2015**, *137*, 8509–8520. (d) Schuster, G. B.; Schmidt, S. P.; Dixon, B. G. Photochemistry of N,N -Dimethyldihydrophenazine and Benzoannelated Analogues. Structurally Dependent Excited-State Hierarchy. *J. Phys. Chem.* **1980**, *84*, 1841–1843.
- (17) **Phenothiazine:** Chen, D.-G.; Chen, Y.; Wu, C.-H.; Chen, Y.-A.; Chen, M.-C.; Lin, J.-A.; Huang, C.-Y.; Su, J.; Tian, H.; Chou, P.-T. Phenothiazine Scope: Steric Strain Induced Planarization and Excimer formation. *Angew. Chem. Int. Ed.* **2019**, *58*, 13297–13301.
- (18) **Dibenzoarsepin:** Kawashima, I.; Imoto, H.; Ishida, M.; Furuta, H.; Yamamoto, S.; Mitsuishi, M.; Tanaka, S.; Fujii, T.; Naka, K. Dibenzoarsepins: Planarization of 8π -Electron System in the Lowest Singlet Excited State. *Angew. Chem. Int. Ed.* **2019**, *58*, 11686–11690.
- (19) **COT angle:** Yuan, C.; Saito, S.; Camacho, C.; Kowalczyk, T.; Irle, S.; Yamaguchi, S. Hybridization of a Flexible Cyclooctatetraene Core and Rigid Aceneimide Wings for Multimultimultifluorescent Flapping π Systems. *Chem. Eur. J.* **2014**, *20*, 2193–2200.
- (20) **Acene:** Sun, Z.; Wu, J. Higher Order Acenes and Fused Acenes with Near-infrared Absorption and Emission. *Aust. J. Chem.* **2011**, *64*, 519–528.
- (21) **Photoresponse in crystals:** (a) Naumov, P.; Karothu, D. P.; Ahmed, E.; Catalano, L.; Commins, P.; Halabi, J. M.; Al-Handawi, M. B.; Li, Liang. The Rise of the Dynamic Crystals. *J. Am. Chem. Soc.* **2020**, *142*, 13256–13272. (b) Hoshino, M.; Uchida, E.; Norikane, Y.; Azumi, R.; Nozawa, S.; Tomita, A.; Sato, T.; Adachi, S.; Koshihara, S. Crystal Melting by Light: X-ray Crystal Structure Analysis of an Azo Crystal Showing Photoinduced Crystal-

- Melt Transition. *J. Am. Chem. Soc.* **2014**, *136*, 9158–9164. (c) Gao, M.; Lu, C.; Jean-Ruel, H.; Liu, L. C.; Marx, A.; Onda, K.; Koshihara, S.-y.; Nakano, Y.; Shao, X.; Hiramatsu, T.; Saito, G.; Yamochi, H.; Cooney, R. R.; Moriena, G.; Sciaini, G.; Miller, R. J. D. Mapping molecular motions leading to charge delocalization with ultrabright electrons *Nature* **2013**, *496*, 343–346. (d) Yamada, T.; Kobatake, S.; Muto, K.; Irie, M. X-ray Crystallographic Study on Single-Crystalline Photochromism of Bis(2,5-dimethyl-3-thienyl)perfluorocyclopentene. *J. Am. Chem. Soc.* **2000**, *122*, 1589–1592. (e) Harada, J.; Uekusa, H.; Ohashi, Y. X-ray Analysis of Structural Changes in Photochromic Salicylidene-aniline Crystals. Solid-State Reaction Induced by Two-Photon Excitation. *J. Am. Chem. Soc.* **1999**, *121*, 5809–5810.
- (22) **CASSCF(2,2)**: Karadakov, P. B.; Saito, S. Can Anti-Aufbau DFT Calculations Estimate Singlet Excited State Aromaticity?, *Angew. Chem. Int. Ed.* **2020**, *59*, 9228–9230.
- (23) **HOMHED**: Frizzo, C. P.; Martins, M. A. P. Aromaticity in heterocycles: new HOMA index parametrization, *Struct. Chem.* **2012**, *23*, 375–380.
- (24) **NICS(1)_{zz}**: Fallah-Bagher-Shaidaei, H.; Wannere, C. S.; Corminboeuf, C.; Puchta, R.; Schleyer, P. v. R. Which NICS Aromaticity Index for Planar π Rings Is Best? *Org. Lett.* **2006**, *8*, 863–866.
- (25) **ACID**: Geuenich, D.; Hess, K.; Köhler, F.; Herges, R. Anisotropy of the Induced Current Density (ACID), a General Method to Quantify and Visualize Electronic Delocalization. *Chem. Rev.* **2005**, *105*, 3758–3772.

Table of Contents (TOC)

